Influence of span-wise coherence in a cylinder wake on the acoustic radiations

Lars Siegel[1], Guosheng He[2,3], Karen Mulleners[2], Arne Henning*[1]

[1] German Aerospace Center (DLR), Inst. for Aerodyn. & Flow Tech., Göttingen, Germany
[2] Institute of Mechanical Engineering, École polytechnique fédérale de Lausanne (EPFL), Switzerland
[3] Beijing Institute of Technology, China
*Corresponding author: arne.henning@dlr.de

Keywords: aeroacoustics, PIV, causality correlation

ABSTRACT

In the present work the influence of the spanwise coherence of the flow structures on the acoustic emission in the case of cylinder wakes is investigated. For this purpose, the correlation between pressure fluctuations in the far field and velocity fluctuations in the wake of the cylinders of different shapes is determined experimentally by means of the so called *causality correlation*. 2D-2C as well as 2D-3C PIV is applied to determine the velocity fluctuations. The pressure fluctuations in the far field are measured synchronously with microphones. From the temporal and spatial distribution of the correlation results, conclusions are drawn about the dependence between the coherence of the vortex structures convecting downstream of the cylinder and the tonal components in the acoustic signature. Most interestingly, in case of a tapered cylinder geometry the temporal evolution of the correlation function shows an asymmetry, which has not been observed in previous results.

1. Introduction

In previous work, the *causality correlation* technique was mainly used to identify longitudinal flow structures in the near wake of a two-dimensional objects using velocity field measurements in a cross-sectional plane (Henning et al., 2008, 2010, 2013). The results indicated that the span-wise coherence of the coherent flow structures has a significant influence on the sound emission and the correlation results (Henning et al., 2010). The aim of the here presented study is to detect and visualise the influence of span-wise coherence on propagating sound waves emanating from a flow around circular cylinders with span-wise variations of the local diameter. Synchronous PIV and microphone measurements are performed in an aeroacoustic wind tunnel. The velocity fluctuations are recorded in the near cylinder wake. By correlating the velocity and pressure fluctuations, the influence of the span-wise cylinder surface irregularities on the acoustic emission is identified. In particular, the temporal and spatial development of these structures provides an insight into the sound generation mechanism. Analyzing the cross-correlation function between the two variables

enables the identification of flow structures which are part of the noise-generating process (Lee & Ribner, 1972; Ribner, 1969; Schaffar, 1979).
The sample cross-correlation function $S_{p,\Psi}(\mathbf{x},\tau)$ is defined as:

$$S_{p,\Psi}(\mathbf{x},\mathbf{y},\tau) = \frac{1}{N}\sum_{i=1}^{N} \Psi'(\mathbf{x},t_i)p'(\mathbf{y},t_i+\tau), \tag{1}$$

where $\Psi'(\mathbf{x},\tau)$ represents the zero-mean part of a near-field quantity measured at position $\mathbf{x}$ and time t_i, $p(\mathbf{y},t_i+\tau)$ is the pressure fluctuation at position $\mathbf{y}$ at time $t_i+\tau$, with τ representing the differences between the points in time when the pressure and flow quantity are recorded. The number of samples of Ψ is N ($N = 15000$ in the present case). In the following the correlation coefficient is analyzed, defined as:

$$R_{p,\Psi}(\mathbf{x},\mathbf{y},\tau) = \frac{S_{p,\Psi}(\mathbf{x},\mathbf{y},\tau)}{\sigma_\Psi(\mathbf{x})\sigma_p(\mathbf{y})}, \tag{2}$$

with $\sigma_\Psi(\mathbf{x})$ and $\sigma_p(\mathbf{y})$ being the RMS-values of Ψ and p respectively. The cross-correlation function can be regarded as a result from a filtering process for the near-field fluctuations, extracting the parts showing a linear dependency with the far-field pressure fluctuations.

2. Experimental Setup

The measurements were performed in the SAG-calibration unit (fig. 1). This is a small circular wind tunnel with a nozzle size of $0.4\,\mathrm{m} \times 0.4\,\mathrm{m}$. The test section is surrounded by a full anechoic chamber of approximately $9\,\mathrm{m} \times 9\,\mathrm{m} \times 5\,\mathrm{m}$ and is certified by DIN EN ISO 3745:2012-07 in the frequency range from $0.1\,\mathrm{kHz}$ to $20\,\mathrm{kHz}$. The selected flow speed was $U_\infty = 43\,\mathrm{m/s}$.

Cylinders with different span-wise irregularities are investigated. Three clean configurations with a constant diameter of $D = 10\,\mathrm{mm}, 15\,\mathrm{mm}$, and $20\,\mathrm{mm}$ are investigated. The other configurations include: a tapered cylinder with a span-wise linear variation of the diameter from $10\,\mathrm{mm}$ to $20\,\mathrm{mm}$, a cylinder with discrete changes in diameter from $15\,\mathrm{mm}$ to $10\,\mathrm{mm}$ and from $10\,\mathrm{mm}$ to $20\,\mathrm{mm}$, a cylinder with equispaced circular fins, a cylinder with a sinusoidal span-wise variation of the diameter, a cylinder with a helical wire pattern, and a cylinder with bumps (see figure 2). The geometric parameters of the cylinders are selected such that the core or the average diameter is D = $15\,\mathrm{mm}$ and the span-wise wavelength for the repeated irregularities are constant.
The velocity field data are acquired using 2D2C-PIV, measuring 2 velocity components, in selected vertical planes around model mid-span (results not shown here). In addition stereo PIV is conducted in a span-wise oriented plane (fig. 1). CMOS cameras (Type: PCO edge 5.5) with a resolution of $2560\,\mathrm{px} \times 2160\,\mathrm{px}$ are used, placed in a $90°$ angle to each other in case of the stereo setup to capture illuminated particles in forward scattering. Scheimpflug adapters are used in order to align the focal- and image-planes compensating for the inclination between the optical axes and the field of view. The recording frequency of the PIV system is $14\,\mathrm{Hz}$ and a total number of $15\,000$

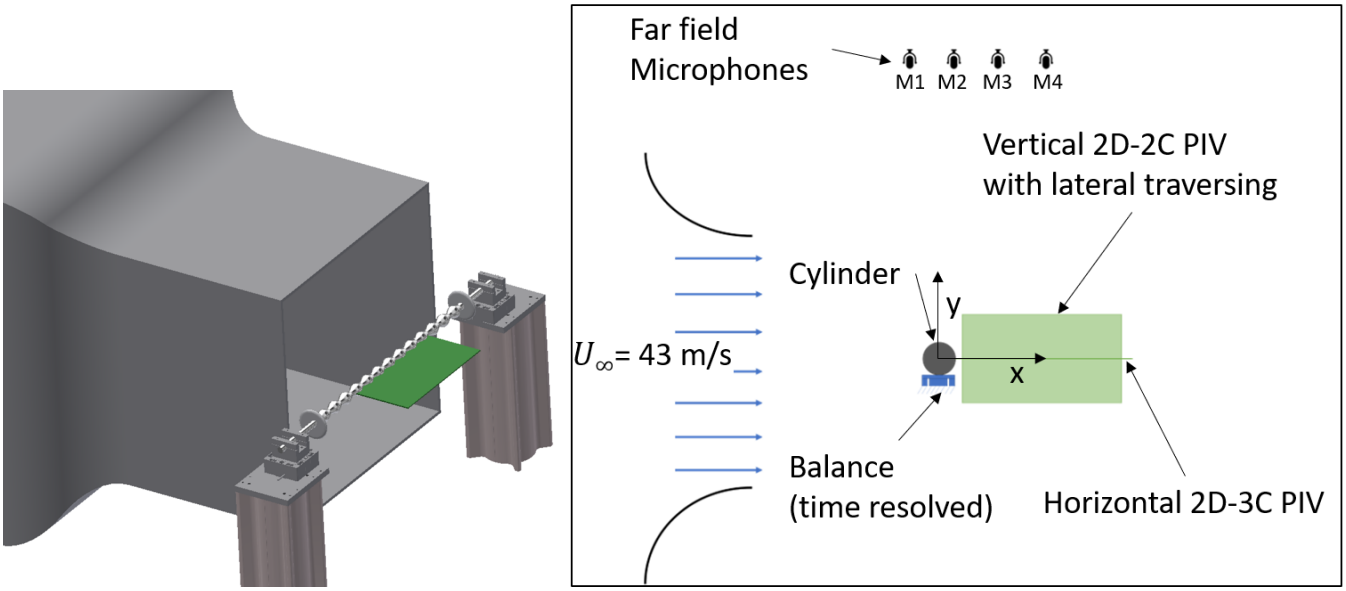

Figure 1. Technical drawing (left) with wind-tunnel nozzle and cylinder mounted in the free stream via the force-balances. Green surface indicated the PIV-plane for the stereo setup. Sketch (right) of the experimental setup (not to scale). Flow from left to right.

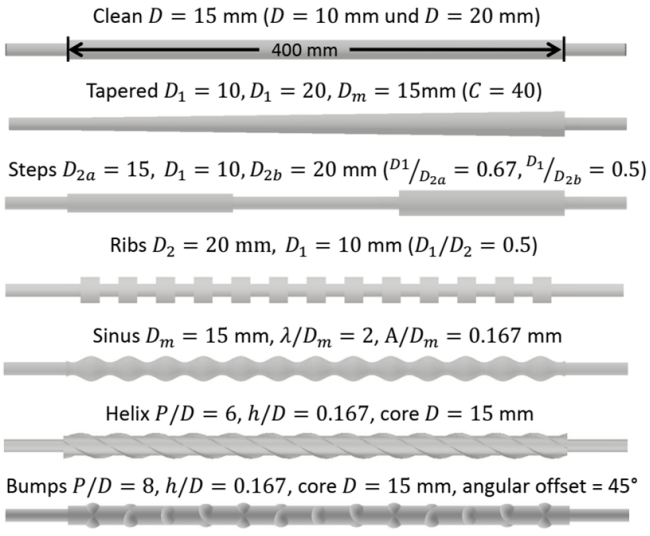

Figure 2. Different Cylinder configurations investigated in the work presented here.

images are recorded for each configuration. The flow is seeded with diethylhexylsebacate (DEHS) tracer particles with a mean particle diameter of approximately $1\,\mu\mathrm{m}$ (Raffel et al., 2007). The seeding particles are injected from a corner of the wind tunnel upstream of the model configuration in a way that the particles have to pass the complete wind tunnel before they reached the field of view. The DEHS particles are illuminated using a double-pulse laser (Q-switched Nd:YAG; Type: Innolas Spitlight 600) with a maximum energy of $350\,\mathrm{mJ}$ per pulse and a repetition rate of $14\,\mathrm{Hz}$. The PIV data were recorded simultaneously with the microphone data. The trigger signals for the camera exposure and the laser-light emission are recorded to be able to assign the corresponding acoustic data to the respective PIV frames. To minimize reflections and unwanted scattered light,

light absorbing tubes are installed along the beam guidance and the cylinders are black anodized. The pressure measurements are conducted with 4 microphones (Type:1/4 40BF; G.R.A.S.) in the far field outside the flow to avoid unwanted influences on the flow field and vice versa. The microphones are installed above the cylinder and are distributed in a horizontal line at the mid-span of the cylinders in flow direction to take into account the directivity of the sound emission. The vertical positions were approximately $1.8\,\mathrm{m}$ above the cylinder. The microphones are protected by wind shields against potential low frequency fluctuations in the plenum.
The time resolved forces acting on the cylinder are measured by means of two balances (Type: K3D60a50N ;ME-GmbH). They are integrated in the support structure on both ends of the cylinder (see figure 1 (left)).
A multi-analyser (Type: DEWE3; Dewetron) simultaneously records the microphone signals, the camera trigger, the q-switch of the laser with a sampling frequency of $f_s = 100\,\mathrm{kHz}$ and a dynamic range of $24\,\mathrm{bit}$. All channels have an anti-aliasing filter at $f_u = 50\,\mathrm{kHz}$. To reduce the influence of low-frequency wind-tunnel noise on the measured signals, a high-pass filter with a cutoff frequency $f_l = 0.5\,\mathrm{kHz}$ is used.

3. Results and Discussion

A detailed analysis of the forces, velocity fluctuations and far-field pressure fluctuations for all configurations goes beyond the scope of paper presented here. The configurations all induce in a unique way a span-wise perturbation in the wake topology that affects the acoustic signature (not shown here). The step configuration induces strong tonal components associated with cells of periodic vortex shedding with different frequencies. The finned, bumped, and the wavy cylinder with the sinusoidal variation in diameter induce strong three dimensional perturbations in the wake due to the interaction of the span-wise von-Karman vortices with the stream-wise vortices that form at the edges of the fins and around the crests of the waves (Arafa & Mohany, 2019; McClure & Yarusevych, 2016; Chyu & Rockwell, 2002). The helical perturbations further add asymmetry to the wake.
In the following, two selected configurations will be analyzed and compared only, namely the clean configuration with $15\,\mathrm{mm}$ diameter and the tapered cylinder with a span-wise linear variation of the diameter from D = $10\,\mathrm{mm}$ to $20\,\mathrm{mm}$. Figure 3 shows the frequency distribution of sound pressure levels at microphone-position M2 for the two selected configurations. Additionally the spectrum in case of the empty test section with and without flow is depicted in the plots. While the signals in the low frequency range of up to approx. $200\,\mathrm{Hz}$ can be assigned to the wind-tunnel noise, clear signals can be observed in the range above this threshold in case of the cylinders installed in the test-section. In case of the clean configuration a peak at $f_p \approx 700\,\mathrm{Hz}$ can be observed, which corresponds to a Strouhal-Number of $St = (f_p D)/(U_\infty) \approx 0.2$. In case of the tapered cylinder, a clear attenuation of the spectrum can be observed in the range between $350\,\mathrm{Hz}$ and $800\,\mathrm{Hz}$. Assuming a constant Strouhal-Number of $St = 0.2$, this corresponds approximately to the diam-

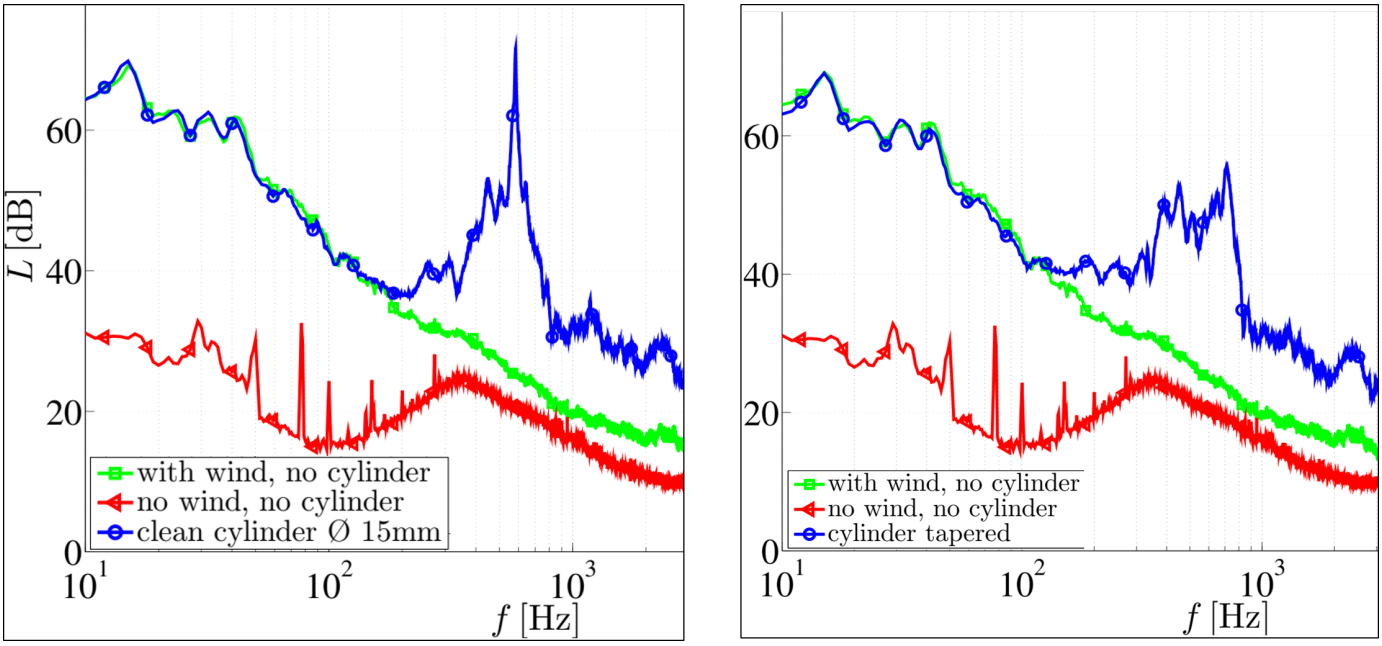

Figure 3. Frequency distribution of sound pressure levels at microphone-position M2 for two selected configurations. The microphone M1 is located vertically above the cylinder position. Sound pressure levels are given in dB with a reference pressure $p_{ref} = 2 \times 10^{-10}$ Pa.

eter range of $D = 10\,\mathrm{mm}$ to $20\,\mathrm{mm}$ in case of the tapered cylinder. Figure 4 shows the RMS values σ_v of the velocity component in y direction (normal to cylinder and free-stream velocity) for the two selected configurations, derived from the stereoscopic PIV-results. In case of the clean configuration, maximum values can be observed at $x/d \approx 2$ downstream of the cylinder. In case of the tapered cylinder, the region of maximum values shows a skewnes, corresponding to the decreasing diameter of the cylinder in the z-direction.

Figure 5 shows the spatial distribution of the correlation coefficient $R_{p,v}$ at values of τ corresponding to the overall maximum values of the coefficient. In both cases, the spatial distribution of the correlation values are dominated by the flow structure of the vortices emanating downstream of the cylinders. In case of the tapered cylinder, these regular structures show a inclination and increasing distance of maximum values in x-direction. In Figure 6 the temporal evolution of the correlation coefficient $R_{p,v}$ at the location $x_* = [z/D, x/D] = [0, 3.02]$ is depicted for both configurations. In case of the clean configuration, the results can clearly be explained by means of characteristics of the signals in the near and far field of the flow, mainly the temporal and spatial evolution of the flow structures and the strong tonal component in the far-field pressure spectrum. As can be seen, the temporal evolution of $R_{v,p}$ shows a strong periodicity, which is due to the periodic vortex shedding and the tonal component in the pressure fluctuations in the far field. The envelope decays symmetrically in both τ-directions, with the maximum located at about $\tau = -5ms$. At the given distance of $1.8\,\mathrm{m}$ from the microphone to the cylinder, this corresponds approximately to the sound travel time from the cylinder to the microphone ($1.8\,\mathrm{m}$ / $340\,\mathrm{m/s} \approx 5\,\mathrm{ms}$). Together with results obtained in previous experiments, in case of the clean configuration the following observations and conclusions can be done:

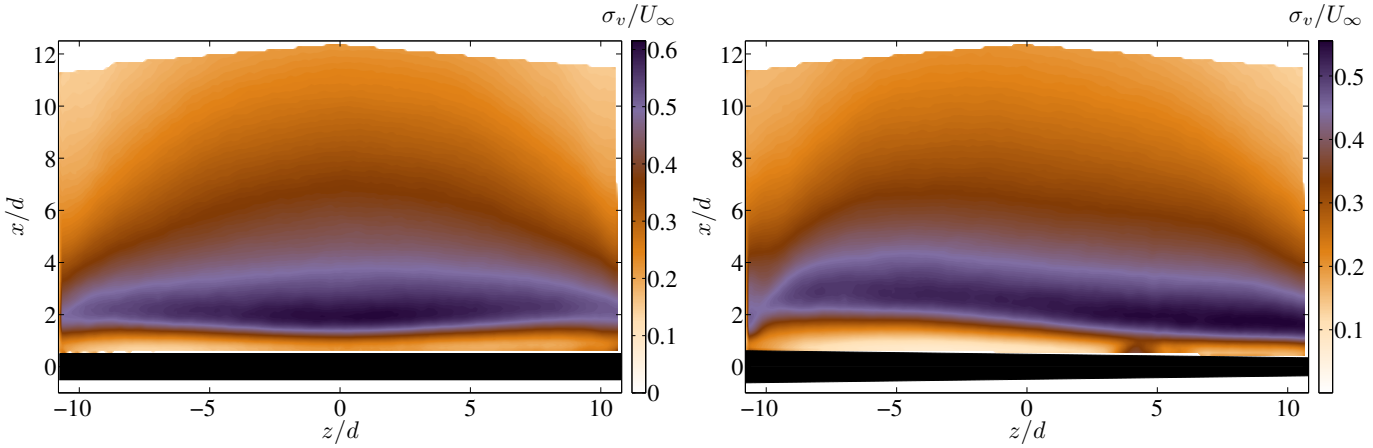

Figure 4. Spatial distribution of the RMS value σ_v of the velocity component in y direction in case of the clean configuration with $D = 15\,\mathrm{mm}$ (left) and the tapered configuration (right).

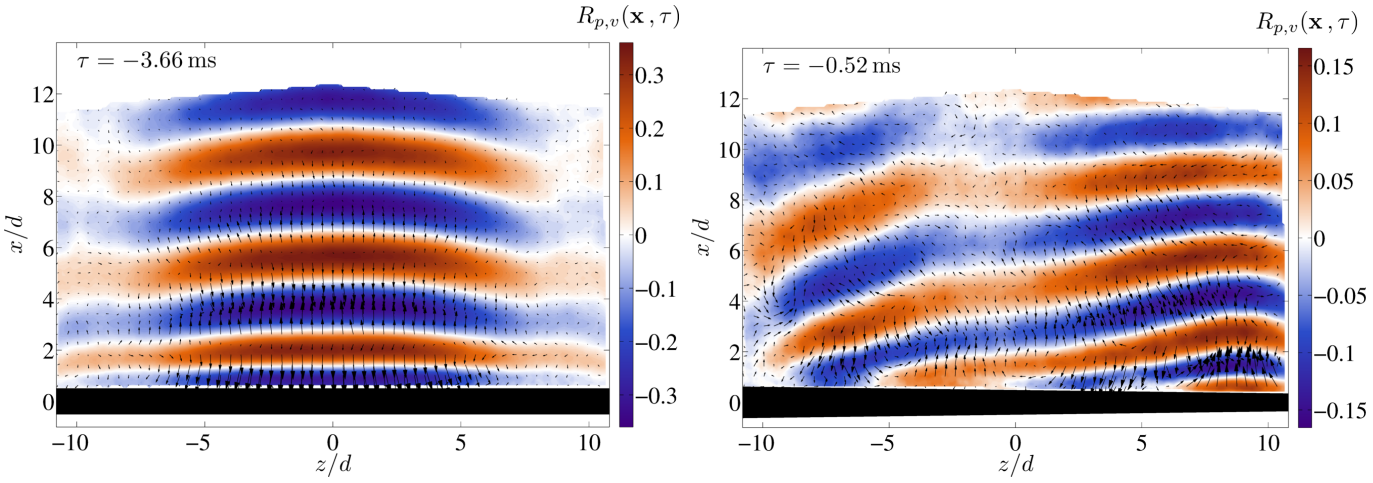

Figure 5. Spatial distribution of the correlation coefficient $R_{p,v}$ color coded at values of τ corresponding to the observation of overall maximum values. The vectors are indicating the values of the correlation between the far-field pressure fluctuations p and the in-plane velocity components in x and z direction [$R_{p,u}$, $R_{p,w}$]. Clean configuration with $D = 15\,\mathrm{mm}$ (left), tapered configuration (right).

- **Periodicity:** If periodic flow structures are responsible for a strong tonal component in the acoustic far field, a periodic time history of the correlation function between the flow fluctuations and the pressure fluctuations in the far field will result. This has been observed, for example, in the case of cylinder wake and a rod-airfoil configuration. In the case of more broadband aeroacoustic sound sources, the correlation function also loses its periodicity and has more the character of a Gaussian modulated sinusoidal pulse.

- **Max location:** If the velocity fluctuation is captured in close vicinity of the actual position of the aeroacoustic sound source, the maximum in the temporal evolution of the correlation coefficient occurs at a value of τ which corresponds to the sound-travel-time from the source to the microphone location. But especially in case strong coherent structures are dominating the flow, the position of the maximum can be observed at shifted values of τ, corresponding

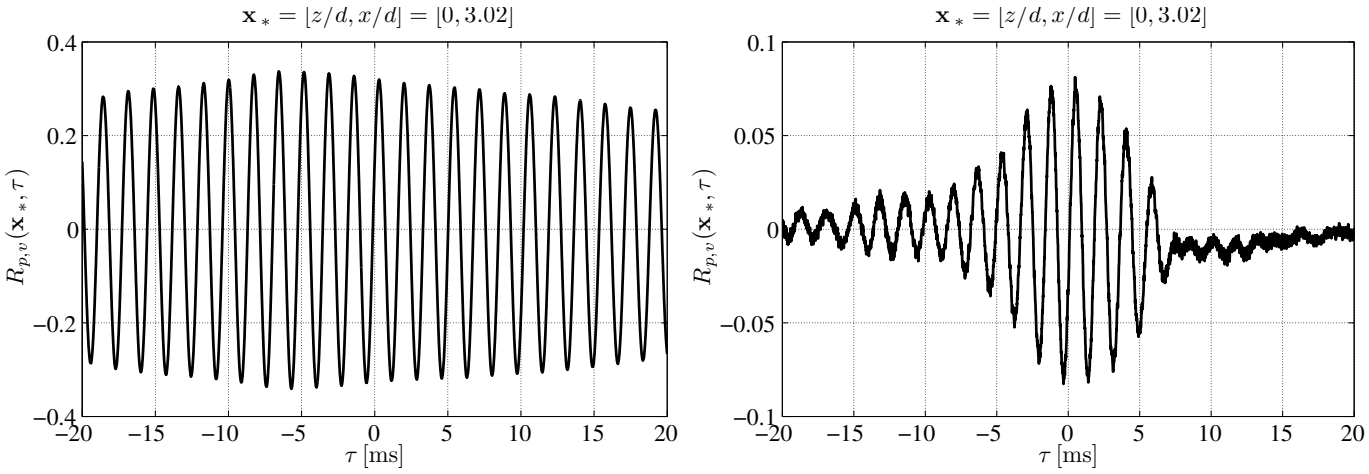

Figure 6. Temporal evolution of the correlation coefficient $R_{p,v}$ at the location $x_* = [z/D, x/D] = [0, 3.02]$. Clean configuration with $D = 15\,\mathrm{mm}$ (left) and the tapered configuration (right).

to the convection velocity of the flow structures. This is true in case these structures in turn correlate with those at the aeroacoustic source position.

- **Symmetry:** The envelope of the correlation function is symmetric around the max location, by means of an equal decrease of the values in positive as well as in negative τ direction. This is especially true in case of strong periodicity of the function.

The same observations were made in the past, where the correlation method has been applied to various generic flow configurations by means of using PIV for capturing the near-field flow variable and microphones for the acoustic emission. While the first observation can be confirmed for the results in case of the tapered cylinder, here the correlation results contradict the observations of maximum position and symmetry. Future work will use the correlation technique to characterize in detail the relation between the far-field pressure fluctuations and the wake topologies behind the different cylinder geometries and the influence of the surface irregularities on the correlation results.

Acknowledgements

This work was supported by the Swiss national science foundation Lead Agency programme under grant number 200021E-169841 and the Deutsche Forschungsgemeinschaft (DFG – German Research Foundation) under grant number HE 7369/2-1.

References

Arafa, N., & Mohany, A. (2019, April). Wake structures and acoustic resonance excitation of a

single finned cylinder in cross-flow. *Journal of Fluids and Structures*, *86*, 70–93.

Chyu, C. K., & Rockwell, D. (2002, February). NEAR-WAKE FLOW STRUCTURE OF A CYLINDER WITH A HELICAL SURFACE PERTURBATION. *Journal of Fluids and Structures*, *16*(2), 263–269.

Henning, A., Kaepernick, K., Ehrenfried, K., Koop, L., & Dillmann, A. (2008). Investigation of aeroacoustic noise generation by simultaneous particle image velocimetry and microphone measurement. *Experiments in Fluids*, *Vol. 348*, 1073 – 1085.

Henning, A., Koop, L., & Ehrenfried, K. (2010). Simultaneous multiplane piv and microphone array measurements on a rod-airfoil configuration. *AIAA Journal*, *44*(48), 2263-2273.

Henning, A., Koop, L., & Schroeder, A. (2013). Causality correlation analysis on a cold jet by means of simultaneous particle image velocimetry and microphone measurements. *Journal of Sound and Vibration*, *332*(13), 3148 - 3162.

Lee, H. K., & Ribner, H. S. (1972). Direct correlation of noise and flow of a jet. *JASA*, *52*(5), 1280-1290.

McClure, J., & Yarusevych, S. (2016, August). Vortex shedding and structural loading characteristics of finned cylinders. *Journal of Fluids and Structures*, *65*, 138–154.

Raffel, M., Willert, C. E., Wereley, S. T., & Kompenhans, J. (2007). *Particle image velocimetry - a practical guide* (2nd ed.). Springer.

Ribner, H. S. (1969). Quadrupole correlations governing the pattern of jet noise. *J. Fluid Mech.*, *38*(1), 1-24.

Schaffar, M. (1979). Direct measurement of the correlation between axial in-jet velocity fluctuations and far field noise near the axis of a cold jet. *J. Sound Vib.*, *64*(1), 73-83.